Usak University

Journal of Engineering Sciences

An international e-journal published by the University of Usak

Journal homepage: dergipark.gov.tr/uujes

Research article

IRREGULAR WAVEMAKER (PISTON TYPE) IN A NUMERICAL AND PHYSICAL WAVE TANK

Bassem Nouioui[1], Mustafa Doğan[2]*

[1] *Civil Engineering Department, Graduate School of Natural and Applied Sciences, Dokuz Eylül University, Izmir, Turkey*

[2] *Civil Engineering Department, Faculty of Engineering, Dokuz Eylül University, Izmir, Turkey*

Received:27 September 2022 Revised: 16 October 2022 Accepted: 24 October 2022 Online available: 30 December 2022
Handling Editor: Jülide Öner

Abstract

This paper describes the design and execution of a wavemaker system (piston type) in the Dokuz Eylül University Hydraulic Laboratory flume to perform hydraulic model tests using regular and irregular waves. In this study, we will focus on generating the irregular waves from the target JONSWAP spectrum using an adjusted random phase method; also, the control software of the wavemaker is described. An identical numerical channel wave to the physical flume was modeled to compare and observe the irregular wave profile using Flow 3D, one of the advanced computational fluid dynamics (CFD) software. The paddle movement was validated by comparing the experimentally converted irregular wave surface elevations to the wave spectrum to the numerical models of several waves.

Keywords: *Wavemaker; random phase method; spectrum; irregular waves; Flow 3D.*

1. Introduction

Hydraulic physical model tests and numerical models are two primary tools for studying wave phenomena (formation transformation and breaking) and solving various coastal engineering problems related to coastal infrastructure planning, design, and construction. Today, hydraulic model tests with irregular waves are generally preferred. For this reason, all laboratories are trying to obtain the types of equipment to produce irregular waves for such tests.

The main advantages of numerical models are that they are readily applicable to large-scale flow fields; they do not necessitate expensive buildings, areas, and equipment; and

*Corresponding author: Bassem Nouioui
E-mail: bassem.nouioui@ogr.deu.edu.tr (ORCID: 0000-0002-2030-4672)

DOI: https://doi.org/10.47137/uujes.1180866

they have a high degree of flexibility in application, adaptation, maintenance, and extension. A numerical model simulated the piston-type wavemaker displacement time series to generate random waves from a target JONSWAP spectrum with Flow3D. Flow3D is a computational fluid dynamics software that enables flow modeling and produces current simulation solutions for engineers who study the dynamic behavior of liquids for physical processes and academic applications.

There are several wave generation techniques in physical models; the most common types are the piston and flap types. The wave generation techniques have been proposed by Goda (2000, Chapter 2), Huges (1993, Chapter 7), Dean and Dalrymple (1984, Chapter 6), and Biésel and Suquet (1951), who theorized the basis for the modern wave generation in hydraulics laboratories. The theory was considerably improved for regular (Fontanet, 1961) and irregular waves (Sand and Mansard, 1986; Schäffer, 1996).

The main objective of this study is to create a deterministic combination of numerical and physical models for coastal waves. Due to the research problem, laboratory conditions, and the high initial investment cost, it is challenging to have a wave channel with an irregular wave generator. Achieving this through imports from Europe or the United States is impossible for some developing countries. The system has been created to generate all forms of regular and irregular gravity waves with domestic capabilities without using expensive types of equipment.

2. Theoretical approach

2.1. Wave spectral analysis

Spectrum analysis is extensively used in the study of noise-like signals because it gives a frequency split into harmonics, the behavior of which may be analyzed independently. It is usual to describe a wave train using its energy. A mathematical formula is frequently used to characterize a wave train's spectrum. Relevant actual recorded wave data under various settings yielded these mathematical calculations. Spectral densities are expressed as a function of variables (such as wind speed and fetch length) or as data defining the sea state (significant wave height H_s and peak frequency f_p). In this study, the JONSWAP spectra S(f) provided by Y. Goda (2000, Chapter 2) in terms of wave height and period parameters is used (eq.1).The JONSWAP is a widely used spectrum in wave estimation applications representing fully-developed sea states and may be expressed as the following :

$$S(f) = \beta_J H_{\frac{1}{3}}^2 T_p^{-4} f^{-5} \; exp\left[-1.25\left(T_p f\right)^{-4}\right] \gamma^{exp\left[-\frac{\left(T_p f-1\right)^2}{2\sigma^2}\right]} \quad (1)$$

In that β_J is a JONSWAP parameter, γ is the spectral shape parameter, $H_{1/3}$ is the significant height, T_p is the peak period, f is the frequency, f_p the peak frequency, and γ is the peak enhancement factor varied from 1 to 7 with a mean value of γ=3.3.

$$\beta_J = \frac{0.0624}{0.230 + 0.0336\gamma - 0.185(1.9 + \gamma)^{-1}}[1.094 - 0.01915 ln\gamma] \quad (2)$$

$$T_p \cong T_{\frac{1}{3}}/[1 - 0.132(\gamma + 0.2)^{-0.559}] \quad (3)$$

$T_{1/3}$ Is the significant period.

□=0.07 □□□ □ ≤□□ □=0.09 □□□ □>□□ (4)

2.2. Random Wave generation

There are two approaches for generating random wave surface profiles from a defined target spectrum: the deterministic spectral amplitude method and non-deterministic spectral amplitude methods. This study calculates waveforms from the JONSWAP spectrum using a deterministic wave generation technique called the Random Phase Method.

After the specification of the energy density spectra of the surface wave profile (target spectrum) and choosing the sampling frequency, the wave amplitude and phase angle associated with a frequency f_n may be obtained from the following:

$$a(f_n) = \sqrt{2S(f_n)\Delta f}$$
$$\varepsilon(f_n) = 2\pi r_N \quad (5)$$

The phase angle ε is arbitrary since it is a random number between zero and one. The choice affects the value of the wave height. However, as long as it is small, this approach gives an excellent random wave profile. The random wave surface elevation is created by superposing linear waves with varying wave heights, periods, and phases; the superposed wave surface elevation is given as the following:

$$\eta(t) = \sum_{n=1}^{N} a(n)\, cos[2\pi f(n)t + \varepsilon(n)] \quad (6)$$

2.3. Time-domain analysis

The zero-up crossing technique is used for time-domain analysis. The wave is characterized when the surface elevation crosses the zero-line or the mean water level (MWL) upward and continues until the next crossing point in the irregular wave time series. The mean water level is determined by averaging the entire water surface profile and defined as the zero line or still water level. A single wave is an event between two consecutive zero-up crossing points (Fig 1). The wave height H is defined as the vertical distance between the highest and lowest points, and the wave period T is the duration between the starting and finishing points of each.

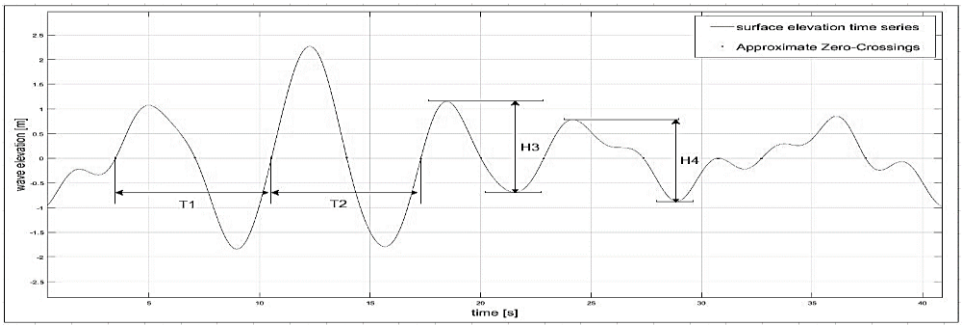

Fig 1. Waves defined by zero-up crossing.

2.4. Random phase method improvement

An example of irregular wave generation is provided with parameters □□ = 7.8□, and □□ = 3.6□. The frequency spectrum type is JONSWAP with □ = 3.3, and Δf=0.001Hz, and the time step is Δ□ = 0.01□. The time series for the water surface profile and its JONSWAP spectrum is given in Fig 2. The theoretical target spectrum is compared to the spectrum obtained from the irregular wave time series in Table 1.

Table 1. Validation of the generated wave with the target parameters.

Parameters	Values from zero-up crossing	Target values
The significant wave height $\boldsymbol{H_s}$ (m)	3.1100	3.6000
Significant wave period $\boldsymbol{T_s}$ (s)	7.3730	7.8000
Peak frequency $\boldsymbol{f_p}$ (Hz)	0,1260	0.1198
Max energy $\mathbf{S}(\boldsymbol{f_p})$ (m^2s)	15.790	22.380

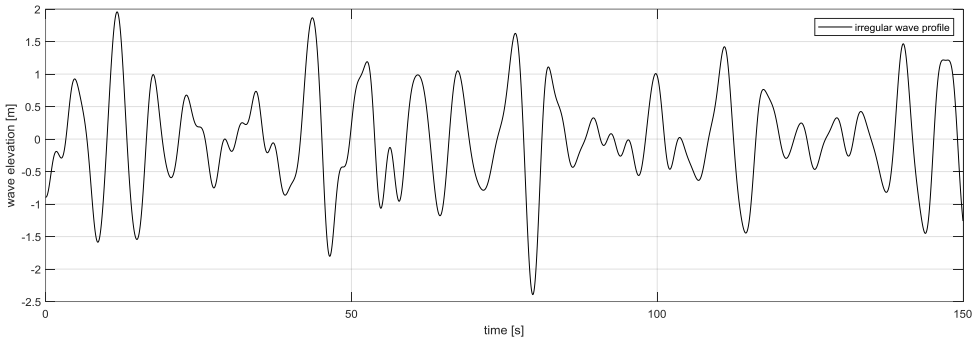

(a) Time series.

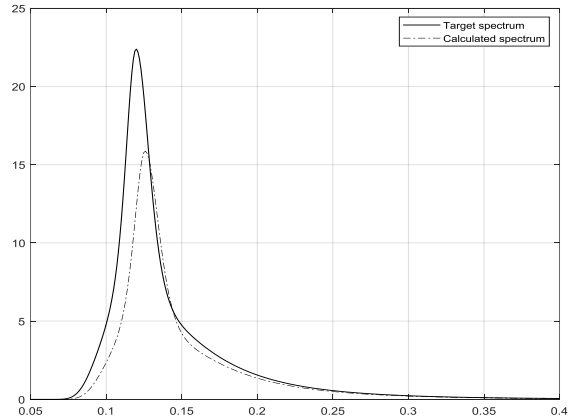

(b) JONSWAP spectrum.

Fig 2. An example of the surface elevation time series of an irregular wave and its JONSWAP spectrum.

To validate the wave generation technique, we suggest a correction factor for the significant height and another for the significant period, which will be sufficient to obtain the target spectrum.

$$CF_{H_s} = \frac{H_{s_{target}}}{H_{s_{calculated}}}$$
$$CF_{T_s} = \frac{T_{s_{target}}}{T_{s_{calculated}}} \quad (7)$$

The wave profile will be adjusted with the following equation:

$$\eta_{adj}(t) = \sum_{n=1}^{N} (a_{cal}(n) \times CF_{H_s}) \cos\left[2\pi f(n)\left(\frac{1}{CF_{T_s}}\right)t + \varepsilon_{cal}(n)\right] \quad (8)$$

Table 2 compares the wave properties from the zero crossing of the adjusted random wave time series and the target spectrum (Fig 3).

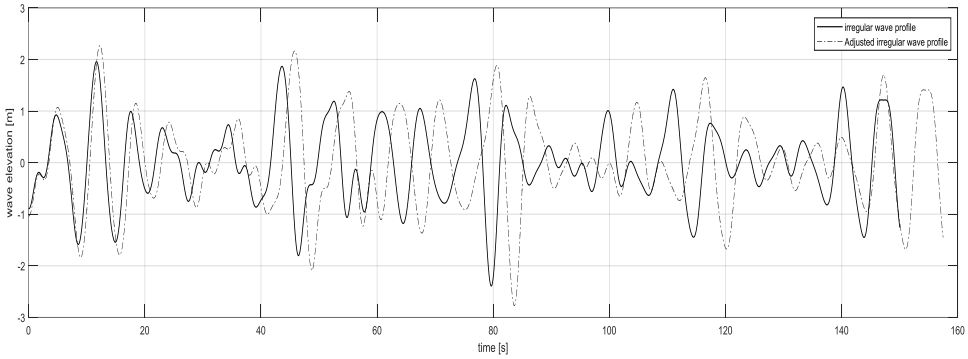

(a) Time series.

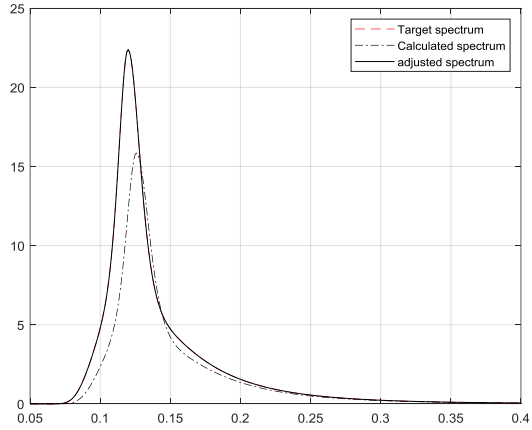

(b) JONSWAP spectrum.

Fig 3. Adjusted surface elevation time series of an irregular wave and its JONSWAP spectrum

Table 2. Validation of the adjusted wave with the target parameters.

Parameters	Values from adjusted time-series	Target values
The significant wave height $\boldsymbol{H_s}$ (m)	3.60000	3.6000
Significant wave period $\boldsymbol{T_s}$ (s)	7.7900	7.8000
Peak frequency $\boldsymbol{f_p}$ (Hz)	0,1198	0.1198
Max energy $\mathbf{S}(\boldsymbol{f_p})$ (m^2s)	22.3800	22.3800

According to the data in Table 2 and as indicated in Fig 3, the target JONSWAP spectrum and the adjusted random wave series are precisely matched, indicating that the random phase method was correctly applied in this study.

2.5. Wave board displacement time series

The target spectrum of the wave paddle motion $S_{paddle}(f)$ is calculated for the target wave spectrum $S(f)$ using equation10. After that, the wave paddle motion (Fig 4) is achieved using Random Phase Method, but by using the same randomly generated phases for the irregular waves. Fig 4 shows a plot of the paddle displacement over the number of data points, which equals to the time of the experiment divided by the sampling rate Δt in seconds.

$$S_{paddle}(f) = S(f)/e_0^2 \tag{10}$$

e_0 is the Biesel transfer function for piston-type wavemaker (eq.11).

$$e_0 = \frac{4\ sinh^2}{2k_0h + \sinh(2k_0h)} \tag{11}$$

Where h is the water depth, and the wavenumber k_0 is the solution to the dispersion relation:

$$\omega^2 = gk_0 \tanh(k_0h) \tag{12}$$

Where g is gravity acceleration, and ω is the angular frequency $(\frac{2\pi}{T})$.

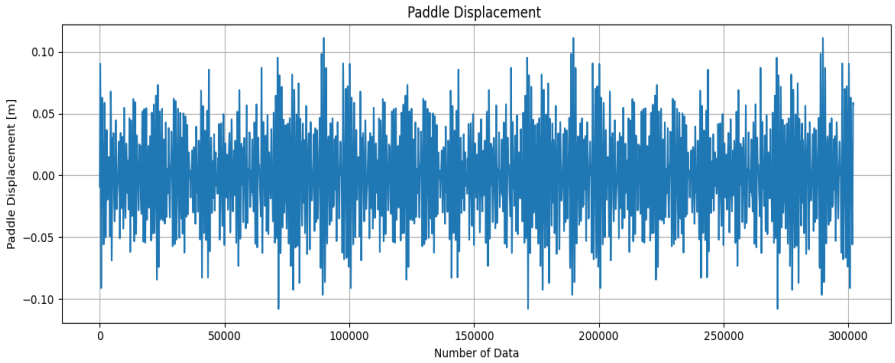

Fig 4. An example of the paddle control signal (H_s=0.144 m, T_s=1.56 s, duration=600 s, and Δt=0.002 s).

Fig. 5 depicts the energy spectra *S(f)* of an irregular wave and the corresponding first-order wave paddle motion $S_{paddle}(f)$.

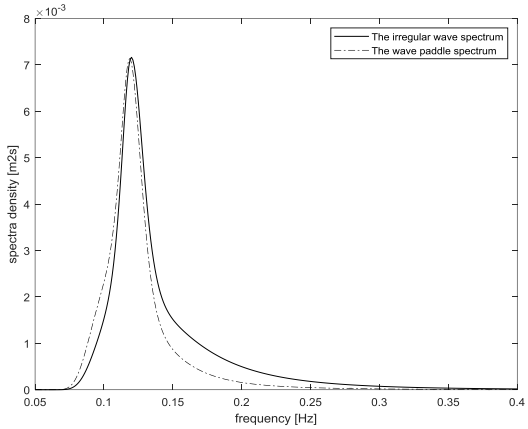

Fig 5. Spectra of the targeted irregular wave and the corresponding first-order wave paddle motion spectrum.

2.6. Preparation of random wave generation signal

In our study, the processing of the input signal to the generator for obtaining irregular waves with the required qualities is typically performed out in line with the flow diagram depicted in Fig 6.

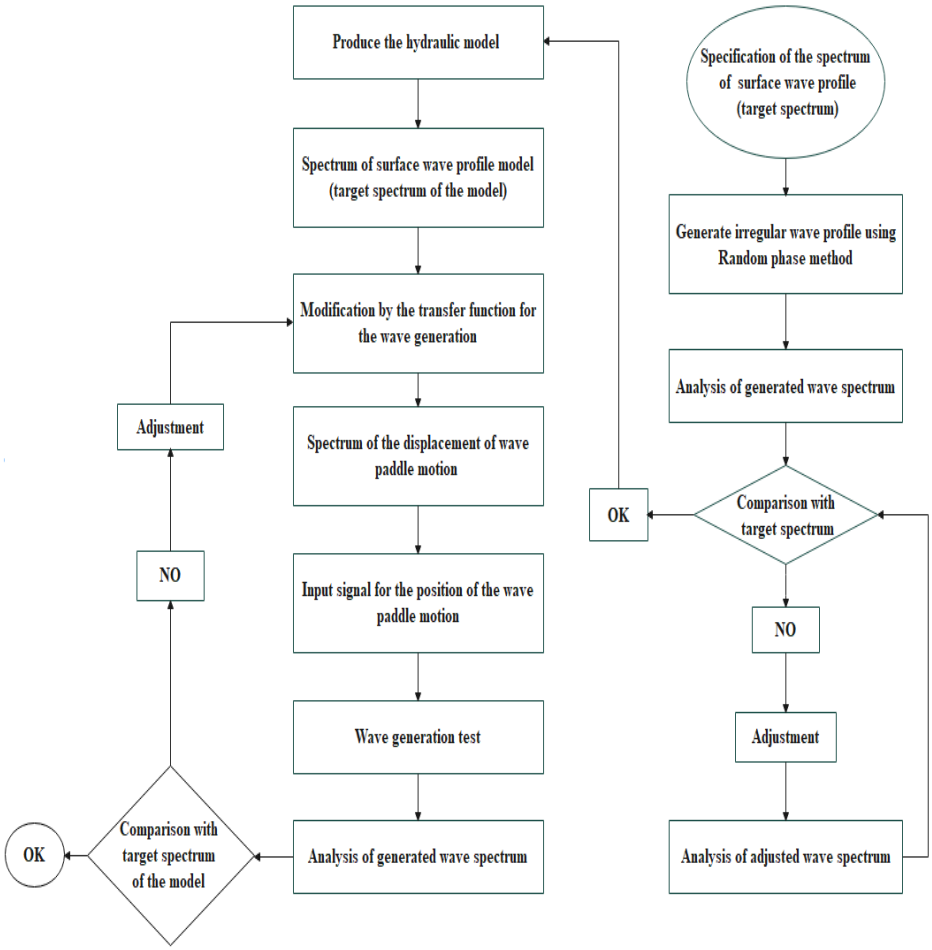

Fig 6. Flow diagram of the preparation of the input signal to an irregular wave generator.

3. Experiment setup

The studies were performed in Dokuz Eylül University Hydraulic Laboratory wave flume, which is 23.4 m long, 1.0 m wide, and 1.2 m deep. One side of the flume is covered with thick glass to allow visual observations during the experiments (Fig 7). A piston-type wave generator is employed to move the water in the flume to achieve the appropriate wave qualities. The wave generator is situated at the beginning of the flume (3m from the offshore side), and two passive wave absorbers are used to avoid wave reflection.

Waves propagate backward on the piston-paddle due to the presence of water on both sides, causing splashes of water that pose a danger of damaging the motor when the created and reflected waves collide. The first absorber is a steel cage packed with absorbent material placed at the back of the generator to absorb wave energy. In contrast, the second absorber is rocks of varying sizes with a slope of 1:7 is installed at the end of the flume.

The experiments were conducted at a constant water depth of d=0.55 m. A servo motor controls the piston, which can create both regular and random waves. The variability of the water surface with time was plotted using two vertical wave probes USS (Ultralab Sound Sensor) positioned during the experiments at the selected measuring points P1 and P2. Two USS20130 sensors at DEU Hydraulic Laboratory were used simultaneously in the experiments within the scope of the study. The sensors are set at a distance of 6 m and 13 m, respectively, from the offshore side. The two sensors were attached to the primary device (ULS Ultralab Level System) with a precision of 1.0 mm and 0.2 s. The data obtained using this device is simultaneously transferred to a computer and stored.

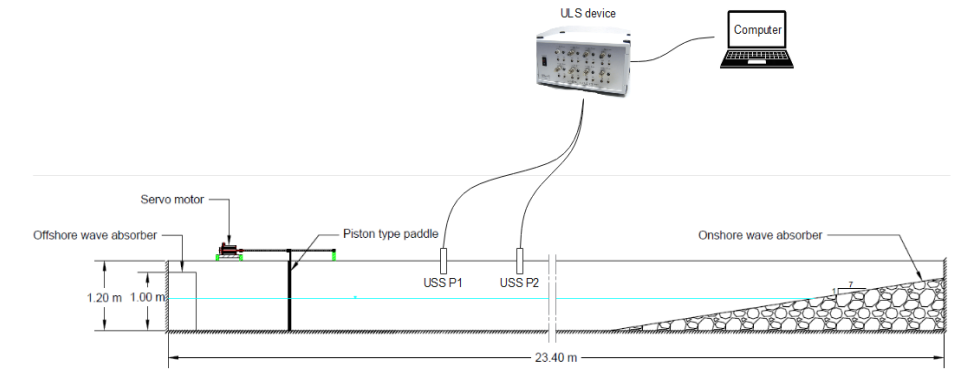

(a) Profile (not to scale)

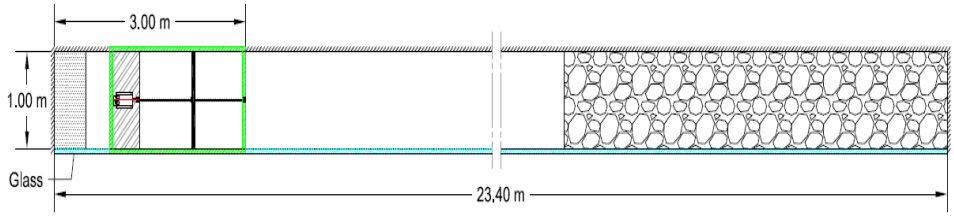

(b) Plan (not to scale)

Fig 7. The wave flume sketch with the measuring equipment.

4. Wavemaker setup

4.1. Mechanical construction

The wavemaker section comprises a stainless steel frame that supports the paddle submerged in the water. The piston-type wavemaker is connected to a ball screw shaft connected to an AC servo motor located at the beginning of the wave flume to create waves (Fig 8 and Fig 9). The rotations of the servo motor are converted into linear motion, which drives the wave paddle back and forth in the wave flume.

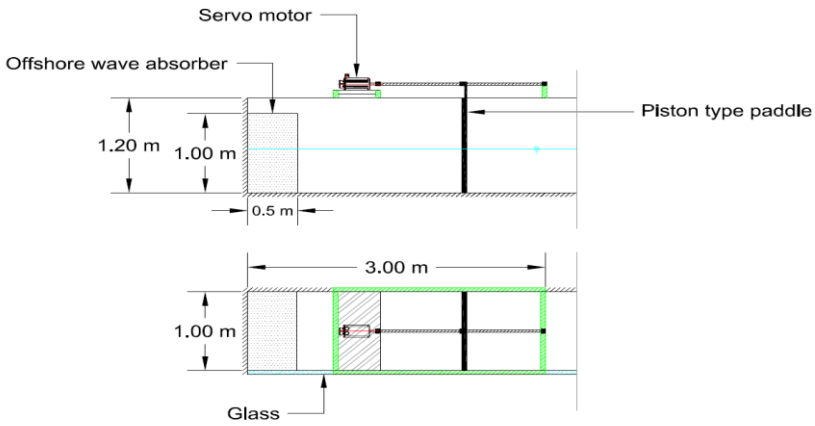

Fig 8. Side and top views of the piston-type wavemaker section design (Not to scale).

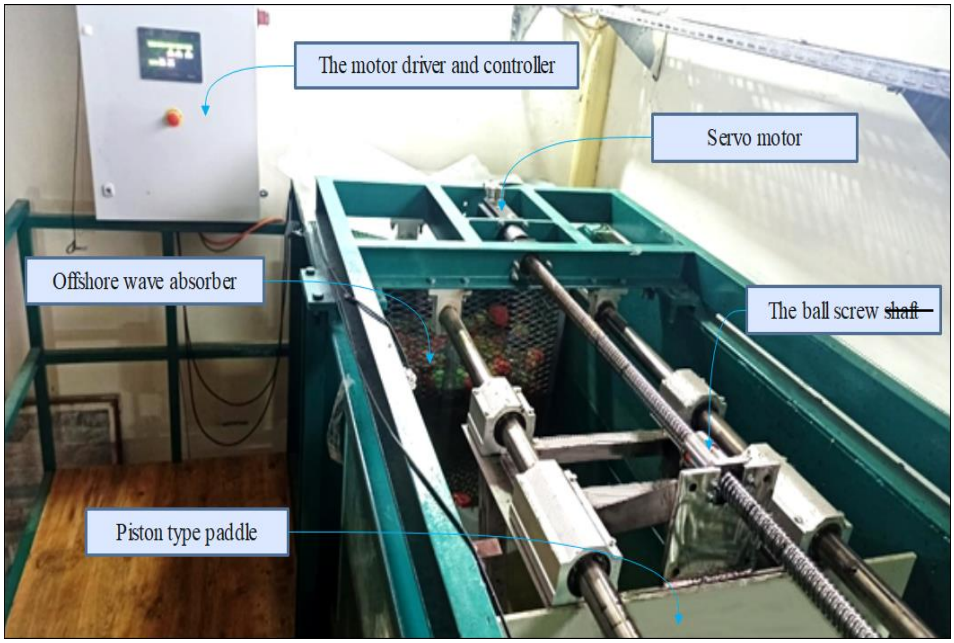

Fig 9. The piston-type wave generator shows the servo motor and ball screw shaft with the motor driver and controller.

4.2. The control software

The wavemaker is controlled by a user program (Fig. 10) written in the Python language and installed on a Personal Computer. The main panel provides information about the wave type (regular or irregular) and its parameters (wave height and period, experiment duration), some buttons are only activated depending on the wave type. After loading the saved results that were previously calculated depending on the type of experiment, the graphs show the paddle movement, surface elevation signals, and the spectrum. By pressing connect to plc button, the PLC will be activated and be ready to receive the input

signal of the paddle displacement from the PC. The servo is activated by pushing the servo On button. In order to protect the paddle from collision at the extremities, the start button that starts the movement of the paddle does not activate until after pressing the home button.

Fig. 10 The user interface of the control software.

5. Numerical approach

The initial configuration of the FLOW 3D simulation is based on the real dimensions of the experiment, so the numerical tank is 23.4 m long, 1 m wide, and 1.2 m tall. The initial water level is 0.55 m. On the offshore side, the wave absorber is defined as a porous component, also 3 m from the offshore side, a solid moving object created to simulate the movement of the piston-type wave generator. However, the wave absorber at the end of the flume is considered a wave absorbing component.

5.1. Geometry creation and model setup

All The simulations were run on a computer with a Core i7 2700-K CPU at 3.40 GHz, 16 GB of RAM. The absorber's geometry was created using SKETCHUP PRO 2021 software. After that, the geometry was converted to stereolithography (STL) file format and loaded into FLOW-3D. The simulation units were set to the international system of units (SI). In the physics of the system, the density is evaluated as a function of other quantities when the Density evaluation tab is selected.

The fluid was one fluid (incompressible) Water at 20 C with all its properties uploaded as the fluid in the fluid properties and set to viscous flow. Also, the RNG model was selected with no slip as the wall shear boundary conditions. The moving objects tab is activated by selecting the "explicit moving" object. The porous media was set to the Darcian saturated drag option.

5.2. Meshing and sensitivity analysis

In this study, the meshing was performed using non-conforming mesh blocks. The mesh cell size was selected to be 0.05m to adopt the hydraulic data outputs and because of the computation time. The sensitivity analysis was pre-checked according to the results of the FAVOR. Fig 11 summarizes the mesh size and the total number of grids. To get better results, the overall model was simulated.

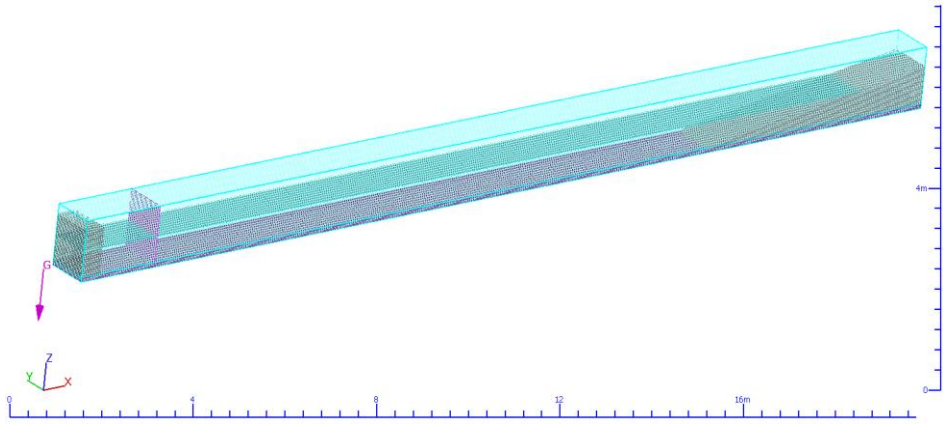

Fig 11. The model mesh system

5.3. Boundary conditions and solution initialization

In this study, the wave generated in Flow 3d used the translational velocity on the x-axis to simulate the movement of a piston-type wavemaker as in the physical model—the top boundary condition z max set to a specified pressure with the fluid fraction equal to 0. While the bottom side (z min), the left side (y min), the right side (y max), the inlet (x min), and the outlet (x max) were set to "wall," as shown in Fig 12.

The slope geometry type was selected as a wave absorber with a damping coefficient of beginning equal to 0 and 1 at the end. The duration of the simulations was set to one hour with a data interval of 0.2 s; the fluid was initialized with an initial fluid elevation of 0.55 m. Finally, the hydraulic data and the fluid velocities were selected at the output tab.

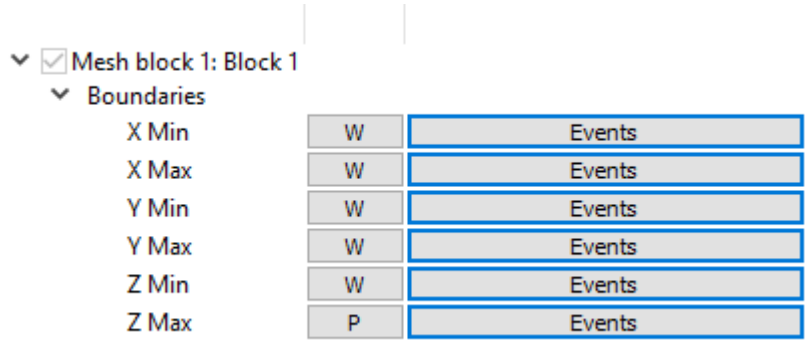

(a) Boundaries conditions.

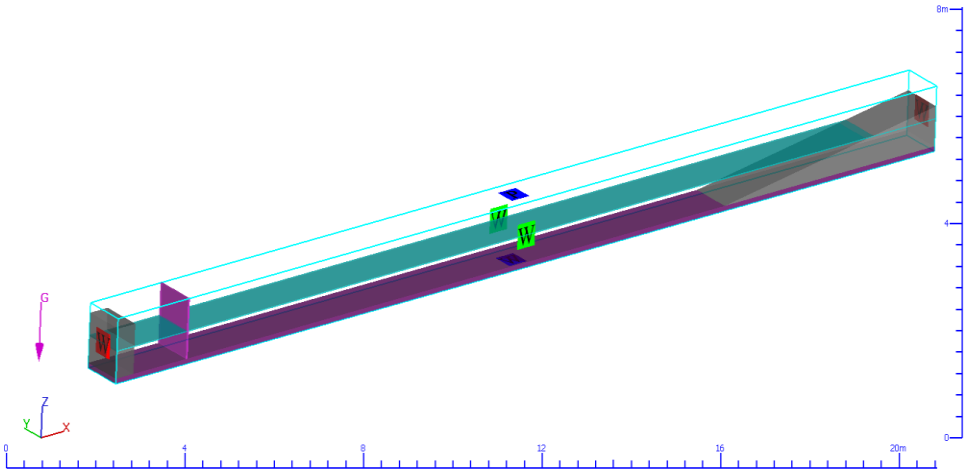

(b) Mesh boundaries.

Fig 12. The Boundary conditions system.

6. Experiment set and results

Within the scope of the study, five experiments and five simulations were performed to test the five wave conditions. The irregular waves (IRW) were generated after specifying the target JONSWAP spectrum. The significant wave heights H_s (0.13 to 0.22 m) and of peak periods T_s (1.56 to 3.6 s) were selected. The spectrum is discretized to N=351 samples. The duration of the experiments was set to 1 hour. The water depth at the paddles of the wavemaker is 0.55 m. The experiment set and the simulation results are summarized in Table 3.

The two sensors (probes), P1 and P2, attached to the ULS are used to obtain the surface elevation of the experiments, which are then used to calculate the wave characteristics using the zero-up crossing method. (and T denote significant wave height and significant wave period, respectively, which corresponds to the mean value of 1/3th of all individual wave heights and periods in the zero-up crossing method, H_{mean} is the mean wave height, H_{RMS} is the root mean square, and H_{max} is the maximum wave height).

- Fig 13 shows two examples of the experimental and numerical surface elevation at P2 of IRW_02 and IRW_04 at P1.
- Fig 14 and Fig 15 show an example of simulated wave profiles.
- Fig 16 to Fig 17 represent the scatter diagram of the experimental and the numerical results.
- Fig 18 to Fig 22 compare the JONSWAP spectrum of the experimental wave (measured H_s and T_s) at the wave gauges P1 and P2 to the theoretical spectrum (Target H_s and T_s).

Table 3. Experiments and set simulation results.

		H_s	T_s	T_p	f_p	H_{mean}	H_{rms}	H_{max}
Target	**IRW 01**	**0.220**	**2.300**	**2.460**	**0.400**	**0.146**	**0.158**	**0.336**
Exp	P1	0.188	2.370	2.540	0.392	0.127	0.139	0.349
Flow 3d		0.216	2.330	2.490	0.400	0.143	0.157	0.346
Exp	P2	0.185	2.297	2.458	0.406	0.1260	0.1380	0.390
Flow 3d		0.189	2.300	2.460	0.400	0.1309	0.141	0.305
Target	**IRW 02**	**0.200**	**2.700**	**2.880**	**0.340**	**0.129**	**0.142**	**0.268**
Exp	P1	0.180	2.730	2.920	0.340	0.112	0.130	0.270
Flow 3d		0.196	2.730	2.920	0.340	0.128	0.141	0.282
Exp	P2	0.190	2.790	2.990	0.330	0.120	0.135	0.317
Flow 3d		0.189	2.820	3.020	0.330	0.128	0.139	0.260
Target	**IRW 03**	**0.170**	**3.100**	**3.310**	**0.300**	**0.110**	**0.121**	**0.255**
Exp	P1	0.1720	2.920	3.130	0.310	0.101	0.119	0.336
Flow 3d		0.1829	3.170	3.400	0.290	0.115	0.129	0.267
Exp	P2	0.169	3.050	3.260	0.300	0.103	0.118	0.320
Flow 3d		0.180	2.980	3.190	0.310	0.111	0.126	0.325
Target	**IRW 04**	**0.130**	**3.600**	**3.850**	**0.259**	**0.084**	**0.093**	**0.178**
Exp	P1	0.133	3.650	3.910	0.255	0.082	0.093	0.187
Flow 3d		0.140	3.610	3.860	0.259	0.087	0.098	0.200
Exp	P2	0.126	3.420	3.670	0.272	0.077	0.087	0.202
Flow 3d		0.141	3.430	3.570	0.270	0.082	0.096	0.237
Target	**IRW 05**	**0.144**	**1.560**	**1.669**	**0.599**	**0.093**	**0.100**	**0.237**
Exp	P1	0.136	1.520	1.626	0.614	0.084	0.100	0.330
Flow 3d		0.139	1.580	1.693	0.590	0.093	0.101	0.237
Exp	P2	0.135	1.520	1.636	0.611	0.088	0.098	0.340
Flow 3d		0.118	1.620	1.740	0.570	0.078	0.080	0.192

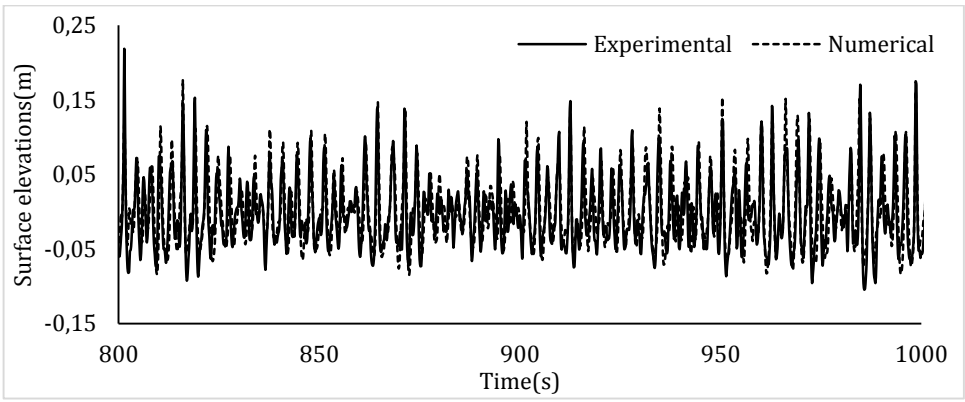

(a) IRW_02_P2

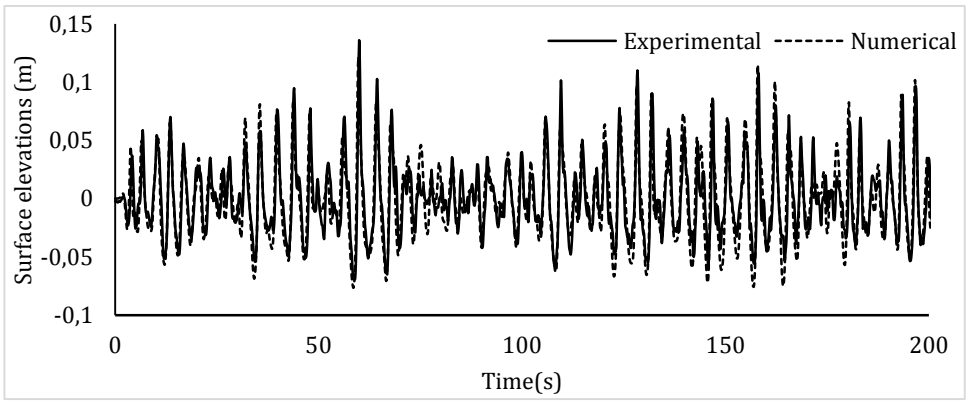

(b) IRW_04_P1

Fig 13. Comparison of the experimental and numerical surface elevations.

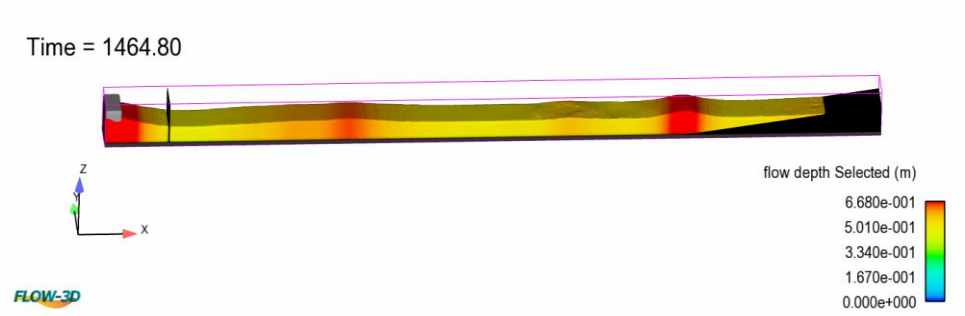

Fig 14. Flow depth example of a simulated irregular wave profile.

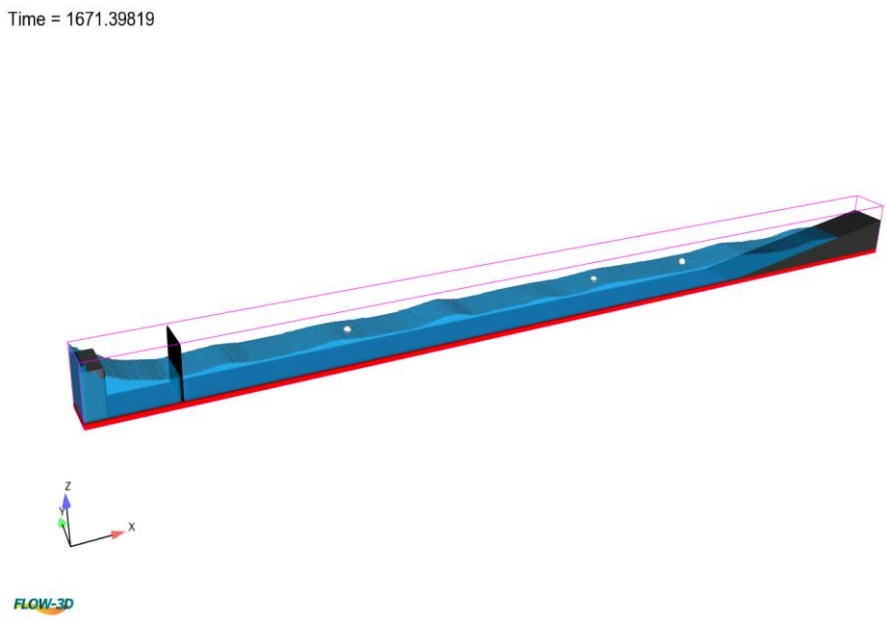

Fig 15. An example of a simulated irregular wave profile.

The errors ratios between theoretical and numerical data (Table 4) and experimental and numerical data (Table 5) are generally less than 10%, except in a few cases (IRW_01_P1, IRW_01_P2, IRW_04_P2, and IRW_05_P2) where the numerical model incorrectly estimates the surface elevations.

The rapid random movement of the paddle (moving object) can cause some unwanted water dispersion, which can lead to more considerable deviation in some cases. Also, the slope shape of the passive wave absorber can behave differently in the experiment due to the variant shape of the rocks, wherein the model was defined as a wave absorber component.

In

Table **6**, the major error ratio between the experimental and theoretical data are 14% for the IRW_01_P1 case and 15% for the IRW_01_P2 case. During the physical experiments, the reflection in the flume distorted the wave record in the case of generating big waves (wave height greater than 0.25m), which affects the wave energy. Some experiment tests were repeated for the validation of the results.

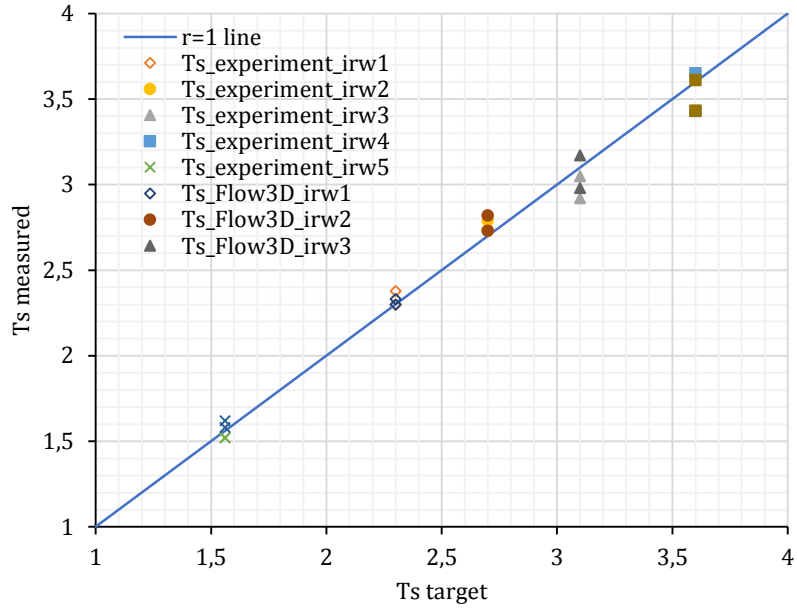

Fig 16. Scatter diagram for experimental and numerical T_s.

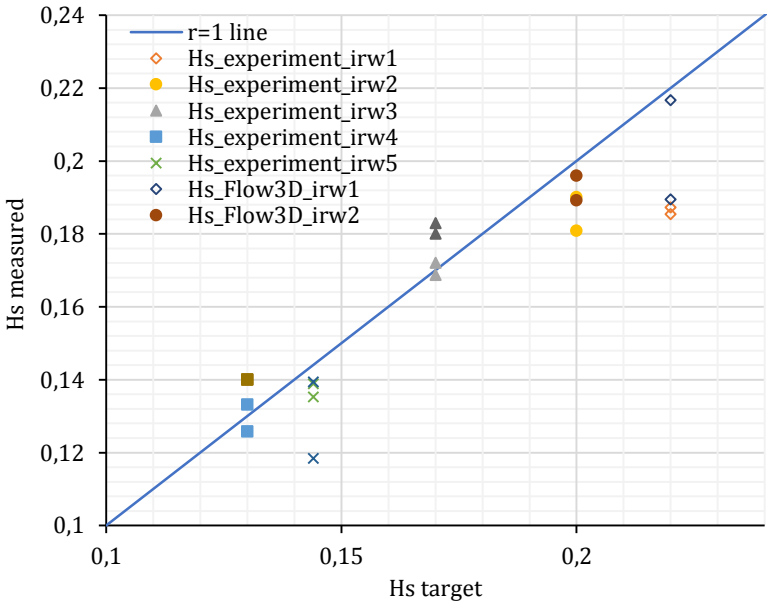

Fig 17. Scatter diagram for experimental and numerical H_s.

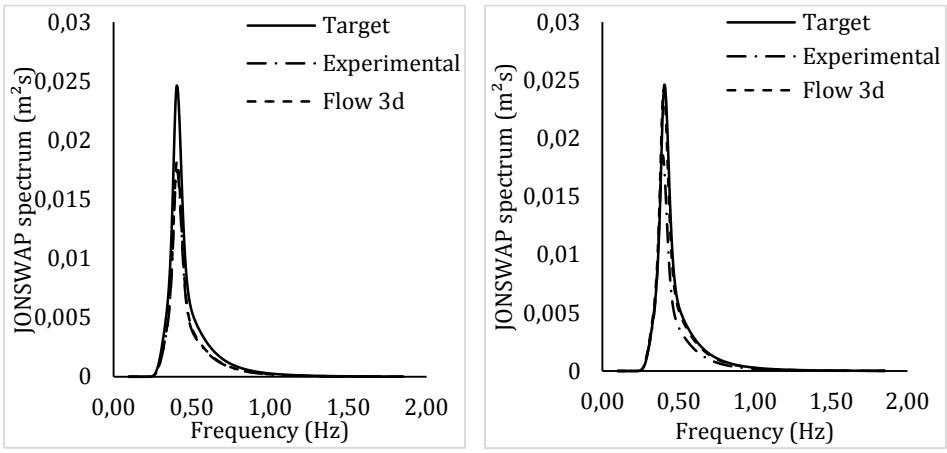

(a) IRW_01_P1 (b) IRW_01_P2

Fig 18. Experimental, numerical, and the target JONSWAP spectrum of IRW_01 H_s =0.22 m T_s=2.3 s.

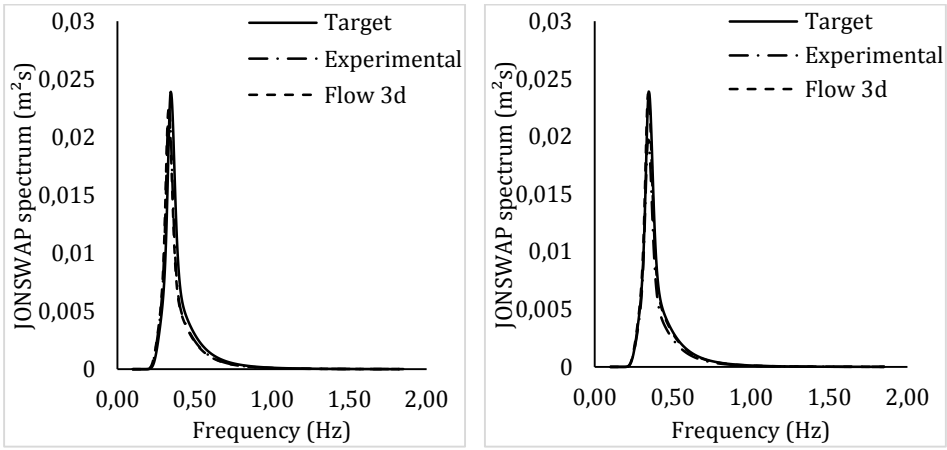

(a) IRW_02_P1 (b) IRW_02_P2

Fig 19. Experimental, numerical, and the target JONSWAP spectrum of IRW_02 H_s=0.20 m T_s= 2.7s.

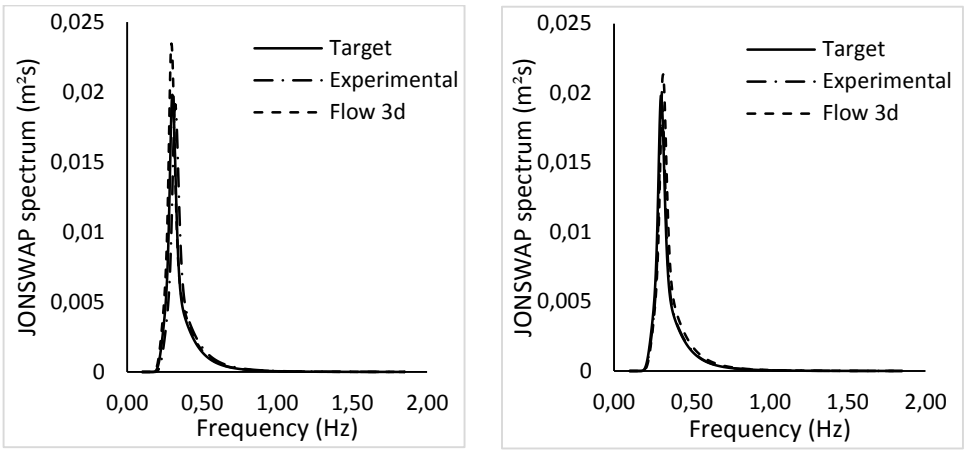

(a) IRW_03_P1 (b) IRW_03_P2

Fig 20. Experimental, numerical, and the target JONSWAP spectrum of IRW_03 H_s=0.17 m T_s=3.1 s.

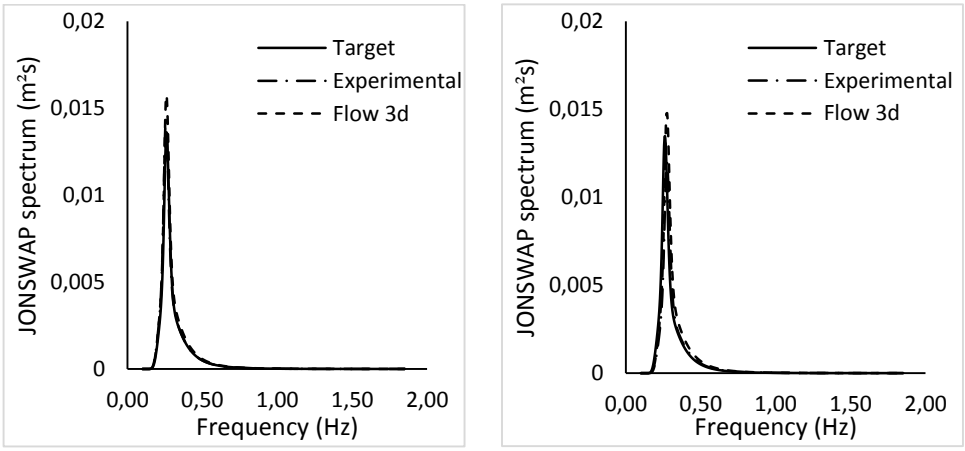

(a) IRW_04_P1 (b) IRW_04_P2

Fig 21. Experimental, numerical, and the target JONSWAP spectrum of IRW_04 H_s=0.13 m T_s =3.6 s.

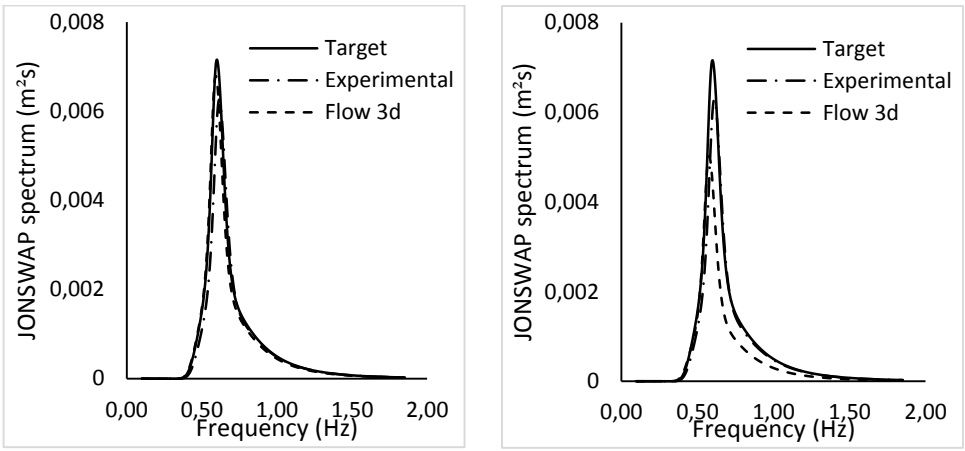

(a). IRW_05_P1 (b). IRW_05_P2

Fig 22. Experimental, numerical, and the target JONSWAP spectrum IRW_05 H_s=0.144 m T_s=1.56 s .

Table 4. Theoretical and numerical data error ratios.

		Error ratios %	
Case name	**Probe**	**H_s**	**T_s**
IRW_01	P1	1.55	1.30
	P2	13.91	0.17
IRW_02	P1	2.30	1.11
	P2	5.40	4.44
IRW_03	P1	7.53	2.26
	P2	5.88	3.87
IRW_04	P1	8.08	0.28
	P2	8.46	4.72
IRW_05	P1	3.19	1.28
	P2	17.78	3.85

Table 5. Experimental and numerical data error ratios

		Error ratios %	
Case name	**Probe**	**H_s**	**T_s**
IRW_01	P1	15.21	1.69
	P2	2.16	0.04
IRW_02	P1	8.56	0.00
	P2	0.42	1.08
IRW_03	P1	6.28	8.56
	P2	6.70	2.30
IRW_04	P1	5.56	1.10
	P2	12.08	0.03
IRW_05	P1	2.20	3.95
	P2	12.43	6.58

Table 6. Theoretical and experimental data error ratios

		Error ratios %	
Case name	**Probe**	**H_s**	**T_s**
IRW_01	P1	14.55	3.04
	P2	15.73	0.13
IRW_02	P1	10.00	1.11
	P2	5.00	3.33
IRW_03	P1	1.18	5.81
	P2	0.76	1.61
IRW_04	P1	2.38	1.39
	P2	3.23	4.75
IRW_05	P1	5.28	2.56
	P2	6.11	2.56

7. Conclusion

In the first part of this study, the irregular wave surface profile was generated from the given target JONSWAP spectrum using the modified random phase method by the correction factors (equation 7). After validating the wave generation technique, user software was developed in Python and installed on a personal computer to control the wavemaker.

The experiments and the numerical model were carried out under identical conditions in the second part. The results obtained from the numerical model were compared with the experimental data. Fig 16 reveals that the experimental and numerical results (significant wave period T_s) were extremely close to the target data. Fig 17 shows that the numerical and experimental error ratios increase when the significant wave height increases.

According to the observations and results of the studies, we can conclude that the wave reflections in the flumes increase the ratio of variances between the target and generated wave characteristics, especially at wave heights greater than 0.25 meters.
Future work in this project will develop a unique shape of passive wave absorption mechanism the wave flume to reduce wave reflection. Future work will also improve waveform computation, control algorithms, and wave-generation precision by developing and testing the second-order transfer function for a piston type irregular wave generator in the wave flume.

Acknowledgment

The authors thank the Scientific and Technological Research Council of Turkey (TUBITAK) for supporting the study by the project 218M445.

References

1. Daoud B, Kobus JM. Irregular wave generation method with given characteristics in experimental tanks. Ocean Eng. 1995;22(4):387–410.
2. Biesel F, Suquet F. Les appareils générateurs de houle en laboratoire. Houille Blanche. 1951;(4):475–96.
3. Dean RG, Dalrymple RA. Water wave mechanics for engineers and scientists. 1984.
4. Eskinja Z, Miskovic I, Androcec V. Modular Wavemaker Design for Harbours and Ships Physical. BroddGradnja. 2008; 59:131–5.
5. Eškinja Z, Mišković I, Fabeković Z. Software for wave generator control. MIPRO 2008 - 31st Int Conv Proc Comput Tech Syst Intell Syst. 2008;3(0):65–9.
6. Frigaard P, Andersen TL. Technical Background Material for the Wave Generation Software AwaSys 5. DCE Tech reports, No 64. 2010;114.
7. Funke E, Mansard E. Laboratory Wave Generation. 1993;333–457.
8. Guillouzouic B. Collation of Wave Simulation Methods. Mar Rep. 2014;1–85.
9. Khalilabadi MR, Bidokhti AA. Design and Construction of an Optimum Wave Flume M.R. 2012;5(3):99–103.
10. Liu Y, Cavalier G, Pastor J, Viera RJ, Guillory C, Judice K, et al. Design and Construction of a Wave Generation System to Model Ocean Conditions in the Gulf of Mexico. Int J Energy Technol. 2012;4(31):1–7.
11. Mišković I, Eškinja Z, Horvat K. Wavemaker control system for irregular developed sea waves generation. 2008 Mediterr Conf Control Autom - Conf Proceedings, MED'08. 2008;791–4.
12. Schäffer HA. Second-order wavemaker theory for irregular waves. Ocean Eng. 1996 Jan 1;23(1):47–88.
13. Schäffer HA, Steenberg CM. Second-order wavemaker theory for multidirectional waves. Ocean Eng. 2003 Jul 1;30(10):1203–31.
14. Schmittner C, Scharnke J, Pauw W, Van Den Berg J, Hennig J. New methods and insights in advanced and realistic basin wave modelling. Proc Int Conf Offshore Mech Arct Eng - OMAE. 2013;5(February).
15. Spinneken J. Wave Generation and Absorption using Force-feedback Control Imperial College London.
16. Wang D xu, Sun J wen, Gui J song, Ma Z, Ning D zhi, Fang K zhao. A numerical piston-type wave-maker toolbox for the open-source library OpenFOAM. J Hydrodyn. 2019;31(4):800–13.
17. Goda Y. Random seas and design of maritime structure. 2000.
18. Zhang H. A deterministic combination of numerical and physical models for coastal waves [Internet]. Orbit.Dtu.Dk. 2005. Available from: http://orbit.dtu.dk/getResource?recordId=195900&objectId=1&versionId=1.